RSC Advances

PAPER

View Article Online
View Journal | View Issue

Check for updates

Cite this: *RSC Adv.*, 2026, **16**, 17207

Synergistic SA/Pebax composite membranes on ceramic supports for efficient ethanol–water separation

Fadias Rara Ardana Lakuy,[a] Taufik Qodar Romadiansyah,[ab] Alvin Rahmad Widyanto,[c] Nur Lailiyah,[a] Resha Mutia Rahma,[a] Riska Amelia,[a] Mikihiro Nomura,[ad] Triyanda Gunawan, [a] Zeni Rahmawati [a] and Nurul Widiastuti *[a]

Efficient ethanol–water separation is vital for sustainable biofuel production, yet conventional techniques remain energy-intensive. This work presents synergistic sodium alginate (SA)/Pebax composite membranes supported on ceramic tubes for high-performance pervaporation. By tuning SA/Pebax ratios (5 : 1 to 3 : 2) and applying glutaraldehyde crosslinking, the membranes exhibit enhanced thermal stability, mechanical strength, and hydrophilicity. FTIR and SEM confirm successful blending and uniform morphology, while AFM reveals controlled surface roughness. Increasing the Pebax composition in the polymer blend improved thermal stability while reducing the swelling degree. Tensile strength tests showed that the 4 : 1 ratio provided a balanced performance, with a tensile strength of 12.04 MPa and elongation of 30.65%. At 50 °C and 90 wt% ethanol feed, the SA/Pebax (4 : 1) membrane achieves a flux of 133 g m^{-2} h^{-1} and a separation factor of 281, raising the separation factor from 5 for pure SA to 281 (56 times). These findings demonstrate that SA/Pebax composite membranes provide opportunities for energy-efficient solutions for water/ethanol separation, aligning with sustainable chemical processing goals.

Received 4th December 2025
Accepted 4th March 2026

DOI: 10.1039/d5ra09375a

rsc.li/rsc-advances

Open Access Article. Published on 30 March 2026. Downloaded on 5/22/2026 11:10:49 PM.
This article is licensed under a Creative Commons Attribution-NonCommercial 3.0 Unported Licence.

Introduction

Ethanol, or ethyl alcohol (C_2H_5OH), is a chemical compound that can be produced through microbial fermentation of carbohydrates derived from various plant-based sources such as corn, sugarcane, wheat, and lignocellulosic biomass.[1] In Indonesia, molasses serve as the principal raw material for bioethanol production. To meet the requirements of its E5 initiative, the nation aims to produce 350 million liters of bioethanol each year.[2] However, fermentation typically yields ethanol at a concentration of only around 10% by weight,[3] thus requiring further purification. This purification process presents a challenge due to the similar molecular sizes of ethanol and water, especially at the azeotropic point of 78.2 °C, which makes separation difficult.[4] Conventional methods such as distillation, extraction, and adsorption face several limitations, including high energy consumption, solvent handling issues, and the generation of environmentally harmful adsorbent waste. Therefore, there is a need for more efficient and environmentally friendly separation methods to sustainably produce high-purity ethanol.

Pervaporation has emerged as a promising alternative for ethanol dehydration. Compared to distillation, pervaporation membranes offer higher selectivity, lower energy consumption, and simpler equipment requirements.[5–7] Additional advantages include minimal pollution, cost-effectiveness, and the ability to separate azeotropic mixtures by overcoming liquid–vapor equilibrium constraints.[8–11] These features make pervaporation an attractive method for organic solvent dehydration. Membrane materials selection determines ethanol production performance. Pervaporation dehydration of ethanol utilizes hydrophilic membranes. Various studies have examined the use of hydrophilic polymers to enhance dehydration efficiency in ethanol–water azeotrope mixtures through the pervaporation method.[12] The most commonly used hydrophilic polymers as membrane materials for ethanol dehydration are chitosan, polyvinyl alcohol (PVA), and sodium alginate (SA). Among these polymers, the SA membrane exhibits the highest flux and selectivity. For example, at 50 °C and 90 wt% ethanol feed, the chitosan membrane demonstrated flux and a separation factor of 240 g m^{-2} h^{-1} and 991, respectively; the PVA membrane produced flux and a separation factor of 260 g m^{-2} h^{-1} and 50, respectively; while SA membrane had flux and a separation

[a]*Department of Chemistry, Faculty of Science and Data Analytics, Institut Teknologi Sepuluh Nopember, Kampus ITS Keputih, Sukolilo, Surabaya, 60111, Indonesia. E-mail: nurul_widiastuti@its.ac.id*

[b]*Department of Chemistry, Faculty of Science and Technology, Universitas Islam Darul 'Ulum, Lamongan, 62253, Indonesia*

[c]*Regional Environment Systems Course, Graduate School of Engineering and Science, Shibaura Institute of Technology, 3-7-5 Toyosu, Koto-ku, Tokyo 135-8548, Japan*

[d]*Materials and Chemistry Program, College of Engineering, Shibaura Institute of Technology, 3-7-5 Toyosu, Koto-ku, Tokyo 135-8548, Japan*

© 2026 The Author(s). Published by the Royal Society of Chemistry

Open Access Article. Published on 30 March 2026. Downloaded on 5/22/2026 11:10:49 PM. This article is licensed under a Creative Commons Attribution-NonCommercial 3.0 Unported Licence.

factor of 290 g m^{-2} h^{-1} and 10 000, respectively.[13–15] Despite these advantages, freestanding SA membranes face challenges, such as low stability,[16] rigid properties,[17] and poor mechanical strength,[18] limiting their practical application. The strong hydrogen bonding between SA molecular chains results in poor flexibility, while the susceptibility of glycosidic bonds to hydrolysis under aqueous conditions leads to stability issues. Furthermore, the absence of a cross-linked network results in inadequate mechanical strength during the pervaporation process.[17,18]

To address these limitations, polymer blending has been widely explored. Previous research has identified the selection and modification of polymeric membrane types to increase selectivity, permeability, and strength, which can enhance the efficiency of the dehydration process.[19] It combines the synergistic properties of different materials into a new composite with improved performance, thereby overcoming the shortcomings of each polymer membrane material.[20] Various current studies on SA-based composite polymer have been developed. Blended SA and polyetherimide (PEI), resulting in flux and separation factor of 1203 g m^{-2} h^{-1} and 1542, respectively.[21] The addition of PEI to SA improved the permeability and stability of the pervaporation membrane in aqueous solutions. However, PEI incorporation reduced water selectivity due to free-volume expansion.[18] Another study involved mixing SA with primary amine-terminated polyamidoamine (PAMAM) to enhance thermal stability. However, it was found that as the number of terminal primary amine groups increased, the interaction between SA and PAMAM dendrimers grew stronger, resulting in a decrease in flux.[22] These findings highlight the need for new composite designs that balance selectivity, stability, and permeability.

Polyether-*block*-amide (PEBA), commercially known as Pebax, is a promising candidate for such blends. Pebax combines the flexibility and permeability of polyether segments with the mechanical strength and thermal stability of polyamide segments.[23,24] Its unique hydrophilic–hydrophobic balance and high water affinity,[25–27] make it suitable for pervaporation membranes. Pebax 1657, which has a polyether (PE)/polyamide (PA) weight ratio of 60/40, was previously used as a polymer blending material with sodium alginate for direct methanol fuel cell applications.[28] Pebax 1657 exhibits a crystalline–amorphous structure that confers thermoplastic and rubber properties to the resulting blend, characterized by high mechanical strength and chemical resistance. This suggests that incorporating sodium alginate and Pebax could be utilized as an ethanol dehydration pervaporation membrane. The integration of SA and Pebax forms ionic cross-links between the acetate groups of sodium alginate and the amide groups of Pebax through electrostatic interactions. Pebax 1657 is a suitable material for blending with sodium alginate because its crystalline–amorphous structure imparts thermoplastic and rubbery properties, yielding high mechanical strength and chemical resistance in the resulting blend.[28] Here in this study introduce a simple and scalable strategy: blending SA with Pebax (polyether-*block*-amide) on ceramic tubular supports with glutaraldehyde (GA) crosslinking to significantly enhance pervaporation performance for water/ethanol separation under energy-efficient conditions.

Integrating selective polymers onto a porous ceramic substrate allows for the creation of organic–inorganic membranes with defect-free surfaces and robust mechanical and thermal durability. In this configuration, the dense polymer coating dictates the separation performance, while the underlying ceramic structure ensures chemical and thermal stability while enhancing overall permeability and ease of processing.[29] The α-alumina ceramic support is a large-pore ceramic substrate suitable for coating with SA/Pebax polymers for ethanol dehydration.[30]

Experimental

Materials

The materials used in this study comprise sodium alginate (HiMedia), polyether-*block*-amide (Pebax 1657, Arkema), α-alumina ceramic support (0.88 μm pore diameter, Iwao Jiki Kogyo Co. Ltd, Japan), demineralized water (Aqua DM), distilled water, hydrochloric acid (HCl, 37%, Sigma-Aldrich), isopropyl alcohol (IPA, ≥99.5%, Sigma-Aldrich), glutaraldehyde (GA, Sigma-Aldrich), and ethanol (99.5%, Merck).

Preparation of SA/Pebax-ceramic membranes

SA was dissolved at 3% (% w/v) in distilled water. Conversely, 3% (% w/v) Pebax was dissolved in an ethanol/water mixture (80/20, % v/v) at 80 °C.[28] Subsequently, SA and Pebax dope solutions were blended in various composition ratios of 5 : 1, 4 : 1, 3 : 2, and 3 : 1 under continuous stirring for 30 minutes. This dope solution was coated onto the outer surface of the commercial ceramic support using the dip coating method for 1 minute and then dried for 12 hours. The dried membrane was immersed in an isopropanol/water mixture (90/10, % v/v), a glutaraldehyde (GA) solution of 5% (% w/v), and 1% HCl (% w/v) for 30 minutes to facilitate crosslinking. Following this, the membrane was rinsed with distilled water and dried further as shown in Fig. 1.

Swelling test

The membrane was dried in a vacuum oven at 40 °C for 12 hours to eliminate residual water. Next, the membrane was weighed

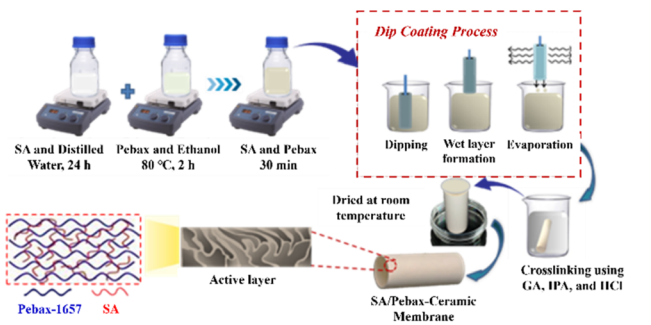

Fig. 1 Scheme of membrane preparation.

© 2026 The Author(s). Published by the Royal Society of Chemistry

Open Access Article. Published on 30 March 2026. Downloaded on 5/22/2026 11:10:49 PM.
This article is licensed under a Creative Commons Attribution-NonCommercial 3.0 Unported Licence.

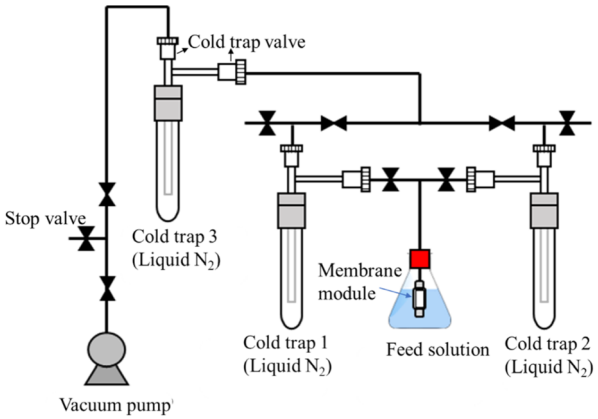

Fig. 2 Pervaporation apparatus model, adopted from previous study.[32]

using an analytical balance (W_D). The dried membrane was soaked in a 90% (w/w) ethanol solution for 16 hours at 50 °C.[31] Then, the membrane surface was cleaned of residual water and weighed again (W_S). The swelling degree (SD%) was determined using eqn (1). The swelling test was repeated three times.

$$\text{SD}\ (\%) = \frac{W_S - W_D}{W_D} \times 100 \quad (1)$$

Pervaporation test

The pervaporation test scheme is shown on Fig. 2. Ethanol dehydration pervaporation tests at 75 °C were conducted using a composite membrane with an SA/Pebax ratio of 4 : 1, which was coated once, twice, and three times on a ceramic support. Subsequently, membranes with SA/Pebax ratios of 5 : 1, 4 : 1, 3 : 1, and 3 : 2 were employed to determine the optimum ratio at 75 °C with a feed concentration of 90%. Additionally, pervaporation tests were performed three times at varying temperatures of 30, 40, 50, 60, and 70 °C and feed concentrations of 50, 60, 70, 80, and 90 wt%. The permeation flux (g m^{-2} h^{-1}) was calculated using eqn (2).

$$J = \frac{Q}{A \times t} \quad (2)$$

where Q (g) represents the mass of the permeate during the pervaporation time t (h), and A (m^2) indicates the effective surface area of the membrane. Gas chromatography (GC) was used to analyze the composition of the feed and permeate. The membrane separation factor (α) can be determined using eqn (3).

$$\alpha = \frac{P_W/P_E}{F_W/F_E} \quad (3)$$

P_A represents the moles of water in the permeate, P_E denotes the moles of ethanol in the permeate, F_A indicates the moles of water in the feed, and F_E refers to the moles of ethanol.

Characterizations

The FTIR spectrometer (Thermo Scientific Nicolet iS10) was utilized for functional group analysis within the range of 500–4000 cm^{-1}. The field emission scanning electron microscope (FE-SEM, JSM-7610F, JEOL) was employed to observe the surface and cross section morphology of the membrane with a potential of 15 kV. Surface topography at the nanometer scale was analyzed using an atomic force microscope (AFM, N8 Neos Bruker). The tensile strength test was conducted to evaluate the mechanical stability of the membrane. The decomposition rate of the membrane as a function of temperature was determined using thermogravimetric analysis–differential scanning calorimetry (TGA–DSC, Hitachi STA200RV). A 3D optical microscope was used for contact angle measurements to assess the membrane's hydrophilicity, and gas chromatography with thermal conductivity detector (GC-TCD, Shimadzu GC-8A) was employed to measure water and ethanol concentrations.

Results and discussion

Membrane structure analysis

FTIR analysis was performed on SA, Pebax, and the blended membranes to identify functional groups and understand the interactions between the two blended polymers by comparing them to the single polymers of SA and Pebax, as shown in Fig. 3.

One of the significant peaks appears at around 3300 cm^{-1}, which is related to the stretching vibration of hydroxyl (–OH) groups.[33] Another peak around 1026 cm^{-1} corresponds to the stretching vibration of the C–O–C group in the glycosidic structure of sodium alginate.[28] The peak near 2926 cm^{-1} is associated with the stretching vibration of the C–H group. The peak shift at 3280 cm^{-1} corresponds to the stretching of the N–H bond in the polyamide group of Pebax.[28] The peak shift around 1110 cm^{-1} is attributed to the C–O–C stretching vibration of the polyether segment, while the peak shift at 1640 cm^{-1} pertains to the amide stretching of the H–N–C=O group within the polyamide. Additionally, several distinctive peaks emerge in the crosslinked SA/Pebax blended, with the 1728 cm^{-1} peak becoming more pronounced, which is caused by the stretching vibration of the carbonyl group of glutaraldehyde. Moreover, the peak around 1630 cm^{-1} is associated with the asymmetric

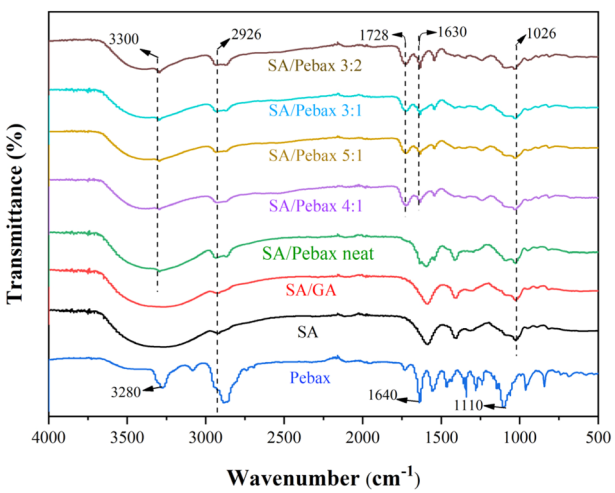

Fig. 3 FTIR spectra of SA/Pebax membrane.

Open Access Article. Published on 30 March 2026. Downloaded on 5/22/2026 11:10:49 PM. This article is licensed under a Creative Commons Attribution-NonCommercial 3.0 Unported Licence.

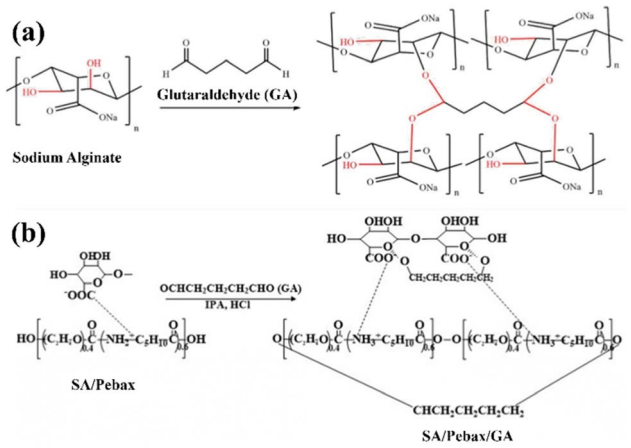

Fig. 4 Schematic illustration of (a) SA/GA and (b) SA/Pebax/GA reaction for synthesized membranes.[28,34]

stretching vibrations of carboxylic groups (COO^-) due to the interaction of SA with glutaraldehyde, as shown in Fig. 4.

SEM analysis provides critical insights into the morphology and structural integrity of the SA and SA/Pebax composite membranes. As shown in Fig. 5, all membranes exhibit a continuous and defect-free selective layer without visible cracks or agglomerates, indicating successful coating on the ceramic support.[35] The pure SA membrane (a.1 and b.1) shows a relatively smooth surface and uniform thickness, but its rigidity and lack of flexibility can lead to brittleness under operational stress.

Upon blending with Pebax, noticeable changes occur in surface morphology and cross-sectional structure. Membranes with higher SA content (5 : 1 and 4 : 1 ratios) maintain a dense and homogeneous layer, while the 3 : 2 ratio exhibits increased roughness and slightly thicker selective layers. This change in thickness can be attributed to differences in the composition and viscosity of the blend solution used during the membrane formation process.[36] This trend correlates with the viscosity of the dope solution: higher Pebax content increases viscosity, resulting in thicker coatings.[37] In addition, the absence of interfacial delamination between the polymer layer and ceramic substrate confirms strong adhesion, which is essential for mechanical stability during pervaporation. The microstructural variations observed are also found to significantly affect membrane performance. An increase in surface roughness associated with higher Pebax content can enhance the effective interfacial contact area; however, excessive roughness may lead to the entrapment of air pockets, thereby adversely influencing the membrane's wetting characteristics.

Membrane surface properties

Water contact angle measurements were performed to evaluate the hydrophilicity of the membranes, and the results are shown in Fig. 6. The SA membrane shows a contact angle of 48°, consistent with literature indicating that pure sodium alginate membrane has a contact angle of 47.82°.[38]

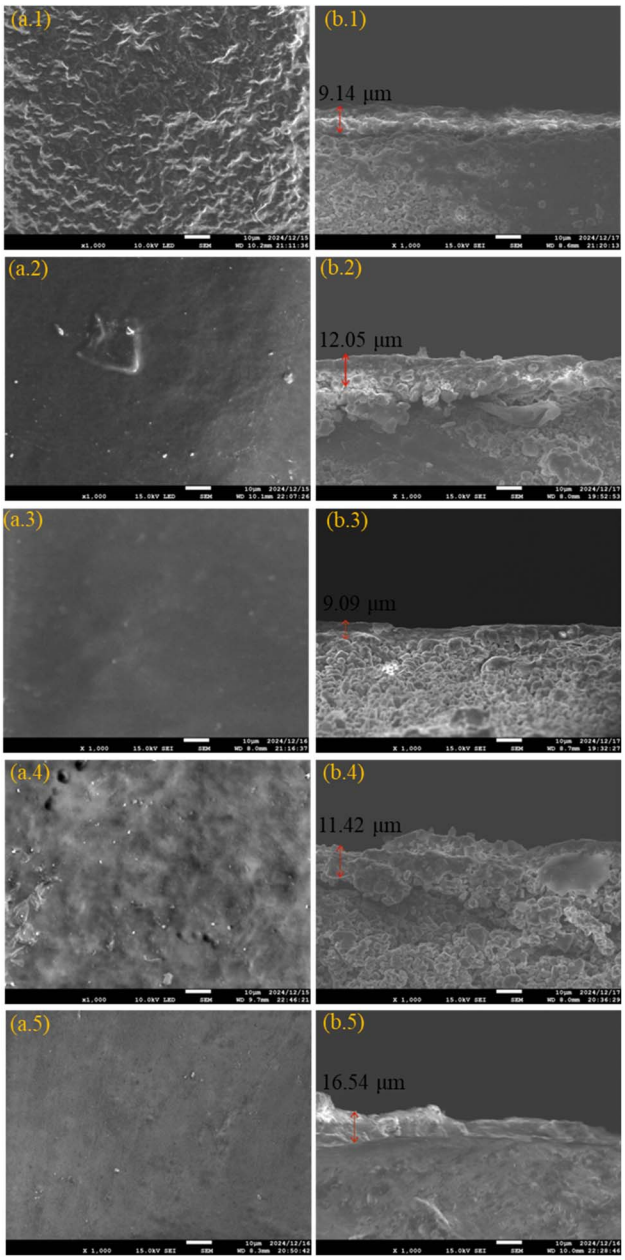

Fig. 5 FE-SEM images of SA and SA/Pebax composite membranes for surface morphology (a) and cross-section (b): (a.1 and b.1) SA and various ratio of SA/Pebax including (a.2 and b.2) 5 : 1; (a.3 and b.3) 4 : 1; (a.4 and b.4) 3 : 1; (a.5 and b.5) 3 : 2, respectively.

Blending SA with Pebax altered the surface hydrophilicity depending on the composition ratio. Membranes with SA/Pebax ratios of 4 : 1 and 3 : 1 showed reduced contact angles of 39° and 45°, respectively, indicating enhanced hydrophilicity compared to pure SA. This slight improvement is attributed to the PE segments in Pebax, which can form hydrogen bonds with water molecules.[39,40] Additionally, Pebax contains hydroxyl groups that further promote hydrogen bonding interactions with water.[41]

Interestingly, when the Pebax content increased to a 3 : 2 ratio, the contact angle rose to 49°, suggesting a slight decrease

© 2026 The Author(s). Published by the Royal Society of Chemistry

Open Access Article. Published on 30 March 2026. Downloaded on 5/22/2026 11:10:49 PM.
This article is licensed under a Creative Commons Attribution-NonCommercial 3.0 Unported Licence.

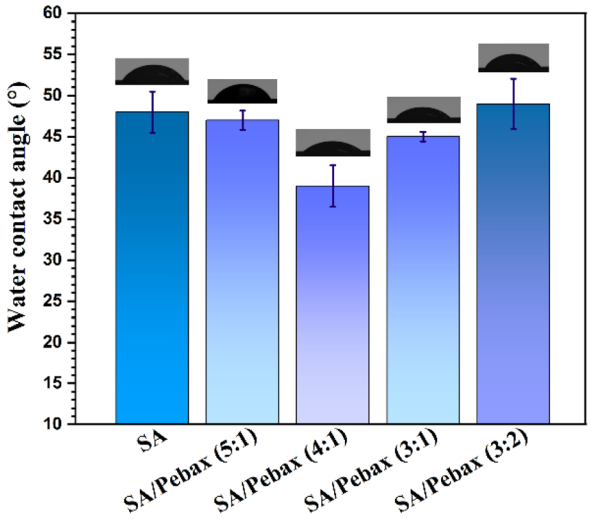

Fig. 6 Membranes water contact angle.

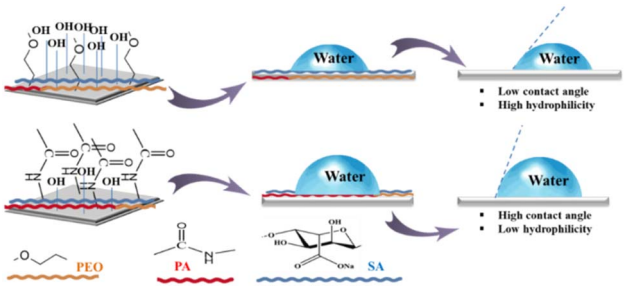

Fig. 7 Effect of SA and Pebax interaction on membrane hydrophilicity.

in hydrophilicity. This reversal is explained by the higher proportion of PA segments in Pebax, which are more rigid and relatively hydrophobic compared to PE segments.[42,43] Thus, the hydrophilicity of SA/Pebax membranes is governed by the interplay between SA's polar groups and the PE and PA segments of Pebax. Fig. 7 illustrates this interaction, highlighting how polymer composition influences surface wettability.

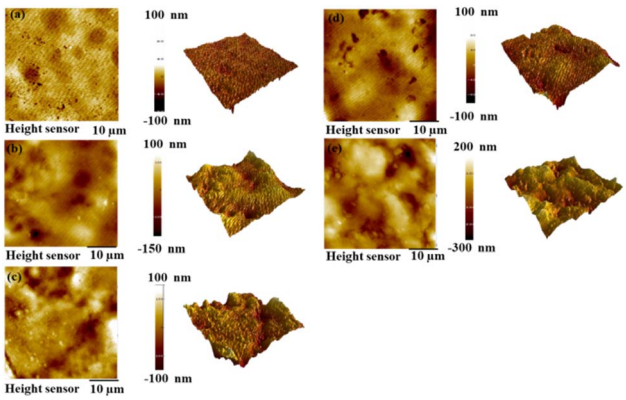

Fig. 8 AFM images of membranes: (a) SA, (b) SA/Pebax 5 : 1, (c) SA/Pebax 4 : 1, (d) SA/Pebax 3 : 1, (e) SA/Pebax 3 : 2.

Table 1 Surface roughness of the membrane

Membranes	S_a (nm)	S_q (nm)
SA	7.3 ± 0.35	9.52 ± 0.57
SA/Pebax (5 : 1)	30.8 ± 8.69	38.9 ± 8.21
SA/Pebax (4 : 1)	27.5 ± 8.70	35.8 ± 4.60
SA/Pebax (3 : 1)	18.8 ± 6.06	24.4 ± 6.73
SA/Pebax (3 : 2)	59.4 ± 4.55	73.9 ± 5.25

Table 2 Mechanical properties of membranes

	Mechanical stability	
Membranes	Tensile strength (MPa)	Elongation (%)
SA/Pebax 3 : 1	11.29 ± 1.40	19.88 ± 1.44
SA/Pebax 3 : 2	10.49 ± 1.15	12.99 ± 1.08
SA/Pebax 4 : 1	12.04 ± 2.11	30.65 ± 1.86
SA/Pebax 5 : 1	12.55 ± 1.98	11.98 ± 0.86

AFM was employed to analyze the surface topography of the membranes at the nanometer scale, as shown in Fig. 8. Surface characteristics at this scale can significantly influence membrane properties such as wettability, permeability, and selectivity, which often differ from bulk behavior.[44] AFM images of the SA membrane and SA/Pebax composites (ratios 5 : 1, 4 : 1, 3 : 1, and 3 : 2) were captured within a 10 × 10 μm scanning area, and the corresponding roughness parameters (S_a and S_q) are summarized in Table 1.

The pure SA membrane exhibited the lowest roughness (S_a = 7.3 ± 0.35 nm, S_q = 9.52 ± 0.57 nm), indicating a smooth and uniform surface. After blending with Pebax, surface roughness increased, suggesting that polymer blending introduces microstructural irregularities due to partial incompatibility or non-uniform distribution during the coating process. Membranes with SA/Pebax ratios of 5 : 1, 4 : 1, and 3 : 1 recorded

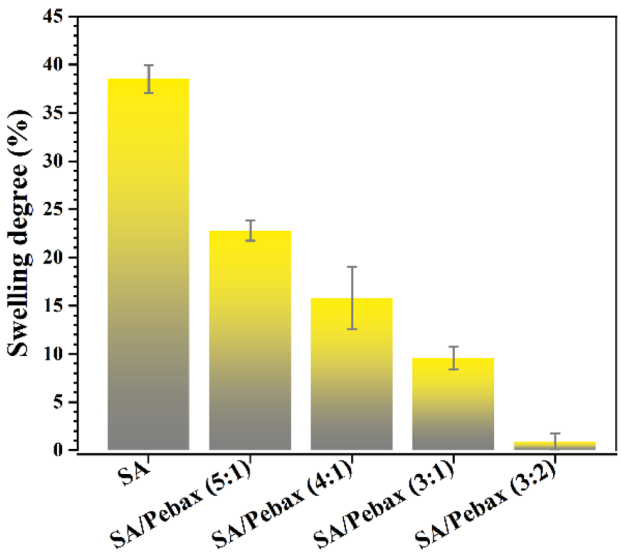

Fig. 9 Swelling test result of the membrane.

Open Access Article. Published on 30 March 2026. Downloaded on 5/22/2026 11:10:49 PM. This article is licensed under a Creative Commons Attribution-NonCommercial 3.0 Unported Licence.

S_a values of 30.8 ± 8.69, 27.5 ± 8.70, and 18.8 ± 6.06 nm, respectively, which correlate with lower water contact angles, consistent with the Wenzel model.[45] According to this model, increased roughness enhances wettability by allowing water to penetrate surface asperities.

However, the SA/Pebax 3 : 2 membrane deviates from this trend. Despite exhibiting the highest roughness (S_a = 59.4 ± 4.55 nm), it also shows the highest water contact angle (49°). This phenomena can be explained by the Cassie–Baxter effect,[46] where excessive roughness traps air pockets within surface cavities, causing water droplets to form more stable spherical shapes and increasing the contact angle. These findings highlight that surface roughness alone does not dictate hydrophilicity; rather, it is the combined effect of roughness and chemical composition (PE *vs.* PA segments) that governs membrane wettability and, ultimately, pervaporation performance.

Mechanical strength of membranes

Mechanical property analysis provides insight into how membranes respond to external stress, which is critical for ensuring durability during pervaporation. As shown in Table 2, the tensile strength of SA/Pebax composite membranes generally decreases as the Pebax content increases. This trend reflects the reduction in rigid SA domains and the introduction of more flexible Pebax segments. Previous studies indicate that lower tensile strength often correlates with increased brittleness due to restricted polymer chain mobility, whereas higher tensile strength and elongation suggest a more flexible and ductile structure.[47] In the present study, the formation of imine bonds between Pebax amide groups and SA acetate groups, along with acetal bonds formed *via* GA crosslinking, restricts chain movement and contributes to stiffness.[28] Among the tested compositions, the SA/Pebax 4 : 1 membrane exhibited the most balanced performance, combining adequate tensile strength

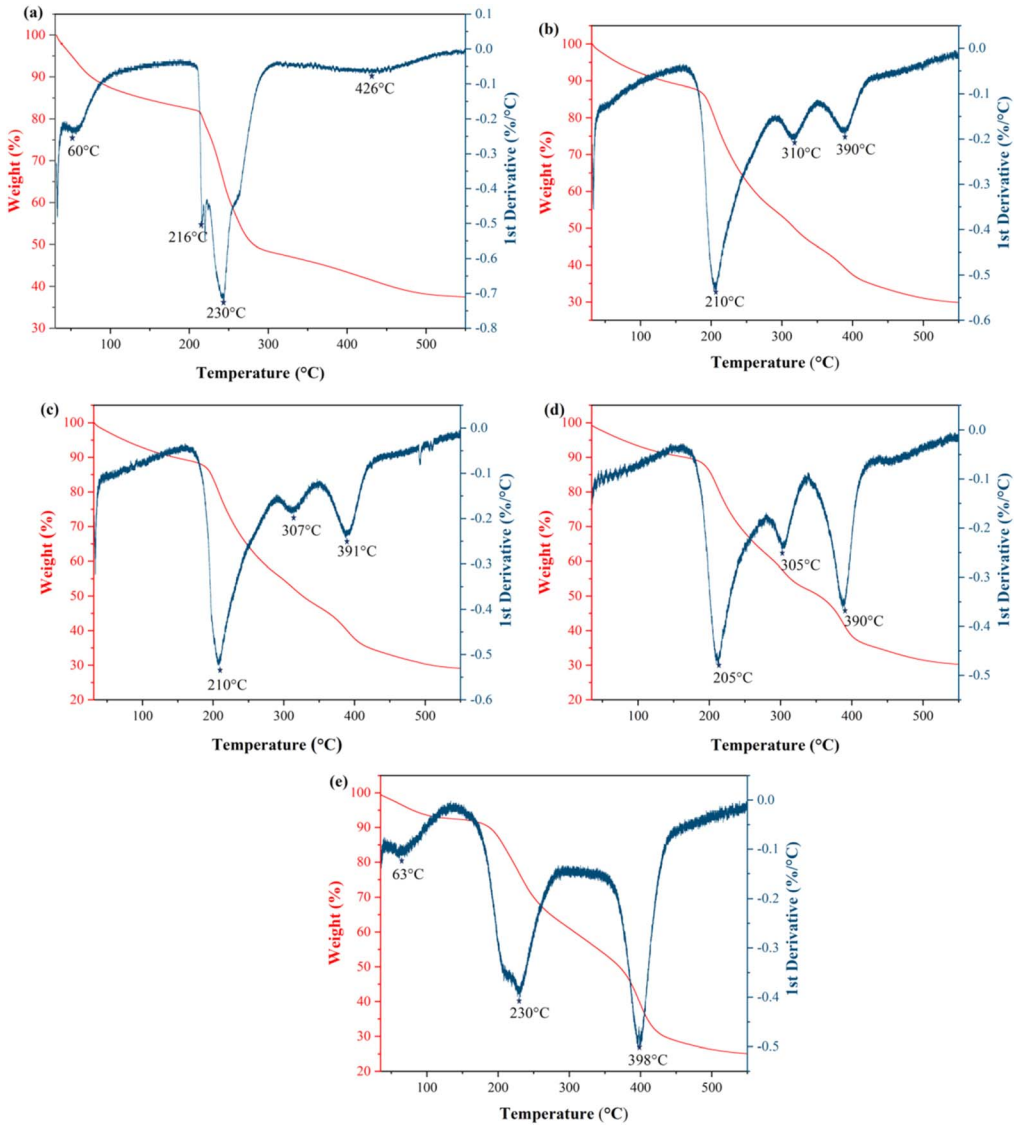

Fig. 10 TGA–DTG curves of membranes: (a) SA; and SA/Pebax with different ratios of (b) 5 : 1; (c) 4 : 1; (d) 3 : 1; and (e) 3 : 2.

© 2026 The Author(s). Published by the Royal Society of Chemistry

Open Access Article. Published on 30 March 2026. Downloaded on 5/22/2026 11:10:49 PM. This article is licensed under a Creative Commons Attribution-NonCommercial 3.0 Unported Licence.

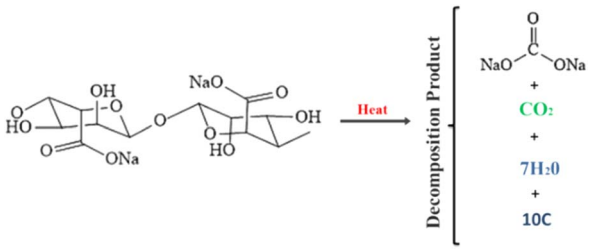

Fig. 11 Sodium alginate decomposition reaction illustration.

(12.04 ± 2.11 MPa) with high elongation (30.65%), which is desirable for operational stability.

Swelling behavior, shown in Fig. 9, further illustrates the importance of structural control. The pure SA membrane exhibited the highest swelling degree (38%), consistent with its strong hydrophilicity. While hydrophilic membranes are essential for water permselective, excessive swelling can lead to polymer plasticization, pore enlargement, and reduced selectivity.[48] This phenomenon compromises separation performance by allowing ethanol to permeate more easily and can also weaken mechanical integrity, increasing the risk of rupture or dissolution during operation. Incorporating Pebax and applying GA crosslinking effectively mitigated this issue, reducing swelling to nearly 0% at an SA/Pebax ratio of 3 : 2. This improvement underscores the synergistic role of Pebax in enhancing structural flexibility and GA in stabilizing the polymer network, ensuring both selectivity and durability under pervaporation conditions.

Thermal properties of membranes

Thermal analysis using TGA–DSC was conducted to evaluate the thermal stability and decomposition behavior of SA membranes and SA/Pebax composites. As shown in Fig. 10a, the initial mass loss near 39 °C corresponds to the evaporation of free water trapped in the membrane.[49] For pure SA membranes, the TGA curve reveals four distinct degradation stages. The first stage, around 60 °C, involves a 10% weight loss due to the removal of hydrogen-bonded water.[50] Subsequent major weight loss (55%) occurs between 216 °C and 230 °C, attributed to glycosidic bond cleavage and pyranose ring decomposition.[50,51] A third stage near 426 °C reflects the conversion of alginate fragments into Na_2CO_3,[51,52] as illustrated in Fig. 11.

Incorporating Pebax shifts degradation temperatures to higher values, indicating improved thermal stability (Fig. 10b–e). For SA/Pebax blends, the first significant degradation stage appears around 210 °C, corresponding to glycosidic bond cleavage and polyether segment breakdown. Subsequent degradation occurs near 300 °C and 390 °C, associated with polyether chain scission and polyamide decomposition. At the 3 : 2 ratio, only two major degradation stages are observed (230 °C and 396 °C), along with minimal initial weight loss (5% at 63 °C) due to free water release.[49] These results suggest stronger intermolecular interactions and a more thermally stable composite structure. The enhanced thermal resistance at higher Pebax content aligns with improved mechanical strength (12 MPa) and negligible swelling, confirming the synergistic effect of Pebax and GA crosslinking.

DSC analysis (Fig. 12) further supports these findings. All membranes exhibit an endothermic transition below 100 °C, corresponding to the glass transition temperature (T_g), where the polymer transitions from a rigid glassy state to a flexible rubbery state.[53] Pure SA shows a T_g near 64 °C, consistent with literature.[50] Pebax® 1657, a PE/PA block copolymer 60 : 40, exhibits a very low T_g (53 °C) for the PE soft segment and 91 °C for the PA hard segment.[54,55] Blending SA with Pebax shifts T_g upward, reflecting restricted chain mobility due to hydrogen bonding between COO^- groups from SA and C=O or –NH groups from Pebax. The melting point (T_m) near 199 °C corresponds to the PE segment, while 230 °C represents SA melting, consistent with TGA observations.[56] These results confirm that SA/Pebax composites offer superior thermal stability and structural integrity compared to pure SA membranes, making them suitable for high-temperature pervaporation applications.

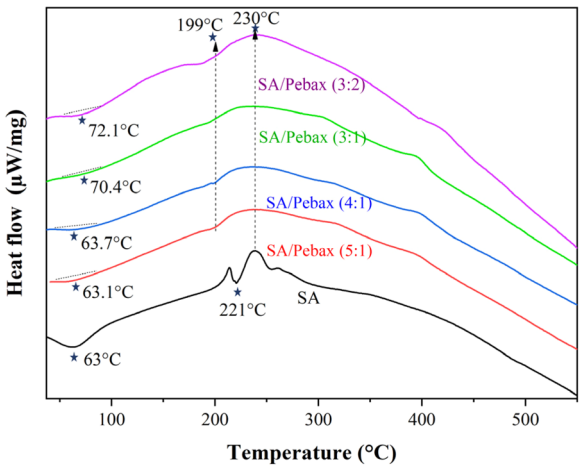

Fig. 12 DSC curves of SA and SA/Pebax composite membranes.

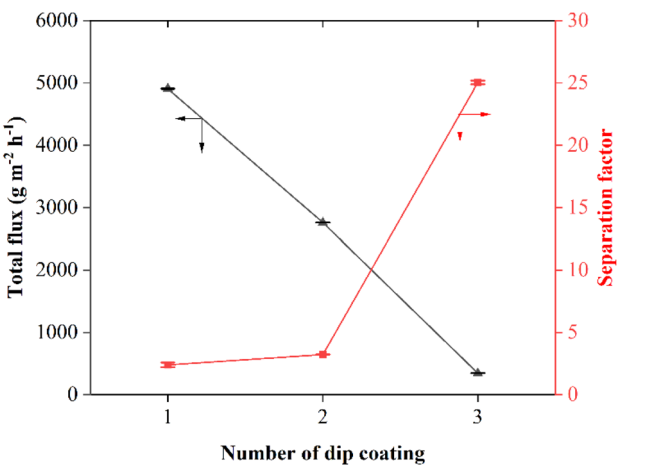

Fig. 13 Effect of dip coating repetition on pervaporation performance.

Open Access Article. Published on 30 March 2026. Downloaded on 5/22/2026 11:10:49 PM.
This article is licensed under a Creative Commons Attribution-NonCommercial 3.0 Unported Licence.

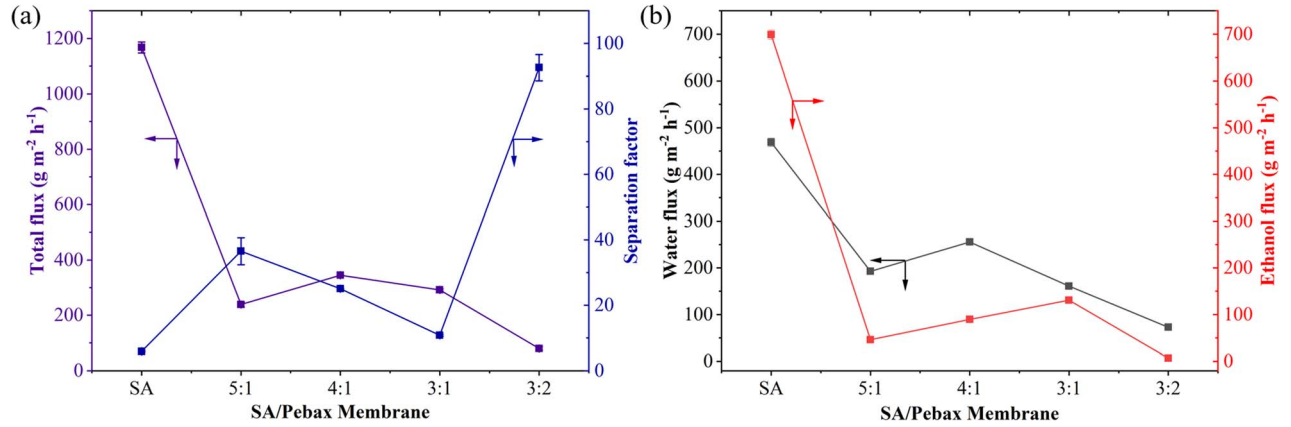

Fig. 14 Effect of SA and Pebax blend ratio on pervaporation performance: (a) total flux and separation factor and (b) water flux and ethanol flux.

Pervaporation performance of ethanol–water dehydration

The pervaporation performance of the varying coating amounts of membrane is shown on Fig. 13. These results align with the literature, which reports that higher fluxes occur at thinner membrane thicknesses.[12] Water and ethanol permeance decreases as the number of membrane coating layers increases, whereas membrane selectivity improves. This behavior is related to sorption and diffusion selectivity, which exhibit a different dependence on the number of membrane layers compared to the overall separation selectivity. Re-coating or adding material can increase the thickness of the selective layer.[57] Repeated coating generally results in a denser structure. This increase in density can reduce the free volume, making it difficult for molecules, especially ethanol, to penetrate. Consequently, it can enhance the selectivity for water.[58] The 3 layer coated membrane exhibits significantly higher selectivity compared to those with fewer coatings; consequently, the evaluation of membrane performance regarding feed concentration and temperature effects was conducted using the 3 layer coated membrane.

The performance results for flux and separation factor are also intrinsically linked to the effective surface area of the membrane. In this study, the effective membrane area used was 8 cm^2. A larger effective membrane area leads to a higher membrane permeation flow rate. The surface area of the tubular membrane corresponds to the ceramic support used. According to the graph presented in Fig. 14, the SA membrane exhibits the highest flux, reaching approximately 1200 g m^{-2} h^{-1}; however, it has a very low separation factor of about 5. When SA is combined with Pebax, the separation factor increases to 93, with a flux of 80 g m^{-2} h^{-1} at an SA/Pebax ratio of 3 : 2. This indicates that incorporating Pebax into the SA membrane composition can enhance the membrane's selectivity for water, despite the lower flux. Pebax consists of polyether and polyamide segments, where the crystalline polyamide segment provides mechanical strength while the polyether segment facilitates the separation process.[59] The SA/Pebax (3 : 2) membrane, which has the highest surface roughness, exhibited a selectivity of 93, aligning with studies indicating that greater roughness generally leads to a more efficient separation area.[60]

Increasing the pervaporation operating temperature raises the permeate flux, as shown in Fig. 15a. The driving force for pervaporation is the difference in partial vapor pressure between the feed and permeate sides. As the feeding temperature rises, the water vapor pressure on the feed side increases exponentially, thereby enhancing the thrust force and

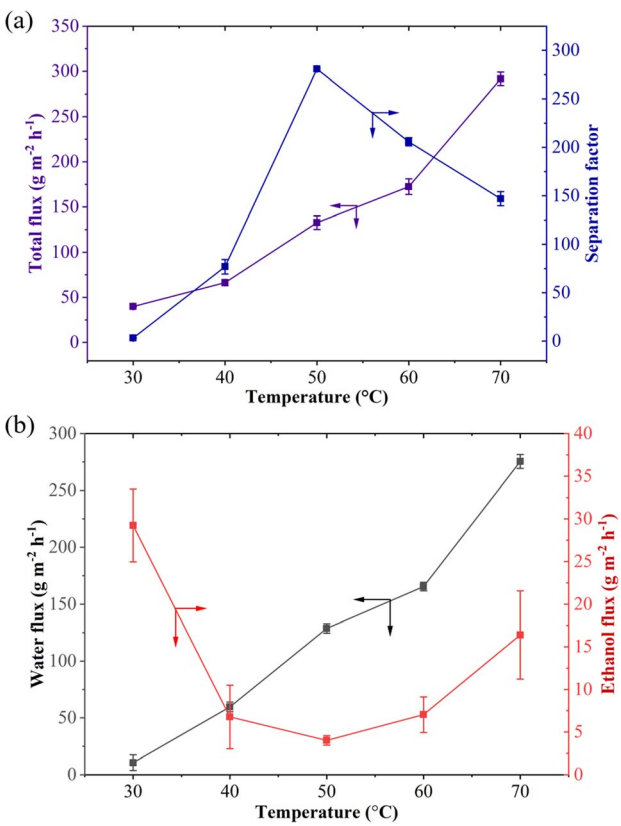

Fig. 15 Effect of operating temperature on pervaporation performance of SA/Pebax (4 : 1) membrane: (a) permeate flux and separation factor and (b) water flux and ethanol flux.

© 2026 The Author(s). Published by the Royal Society of Chemistry

Open Access Article. Published on 30 March 2026. Downloaded on 5/22/2026 11:10:49 PM. This article is licensed under a Creative Commons Attribution-NonCommercial 3.0 Unported Licence.

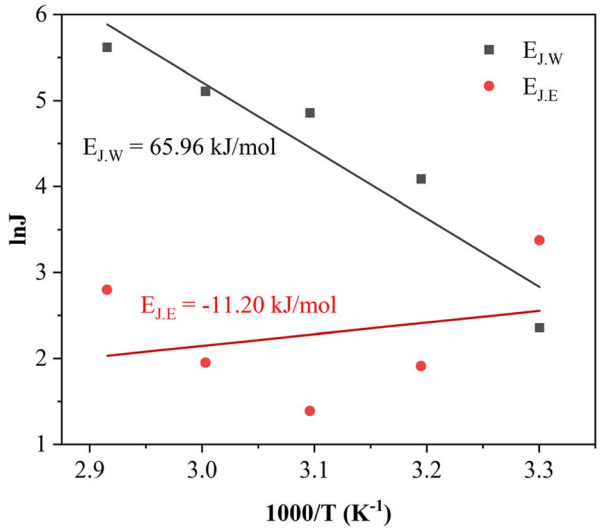

Fig. 16 Arrhenius plots of water and ethanol.

consequently raising the flux. Optimal pervaporation performance is achieved through a balance between permeation flux and separation selectivity. Fig. 15b illustrates that increasing temperature enhances the flux of both water and ethanol, although the flux of water is consistently much greater. Conversely, the separation factor reaches an optimum at 50 °C with fluxes and separation factor of 133 ± 7.52 g m^{-2} h^{-1} and 281 ± 1.11, respectively. This temperature is close to the T_g of the SA/Pebax (4 : 1) membrane, which is 63.7 °C. Pervaporation performance near the T_g allows for sufficient mobility of the SA/Pebax membrane polymer chains, facilitating water transport without excessively reducing selectivity. Temperatures above 50 °C diminish the selectivity of the membrane. More active polymer chain movement at elevated temperatures eases the penetration of solute molecules through the membrane. High temperatures "open" the membrane kinetically, increasing the movement of water/ethanol molecules while mechanically reducing the slight rate difference between the two components, which impacts selectivity.[61]

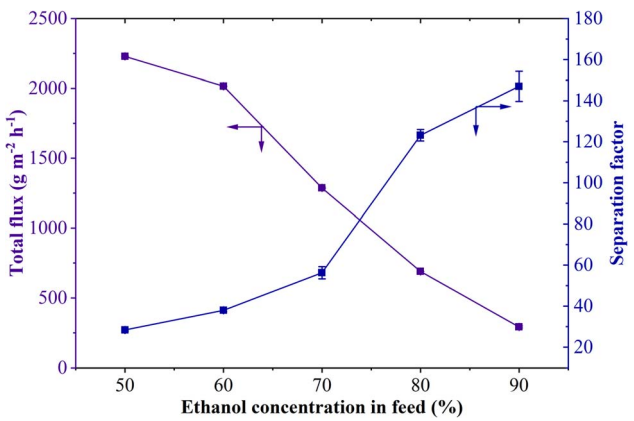

Fig. 17 Effect of feed concentration on the separation performance of SA/Pebax (4 : 1) membrane.

The activation energies for water and ethanol pervaporation were determined using the Arrhenius equation (Fig. 16). The activation energy for water (65.96 kJ mol^{-1}) is notably higher than that for ethanol (−11.20 kJ mol^{-1}). These positive values suggest that the pervaporation process for water is endothermic.[16] Since substances with higher activation energies are more responsive to temperature variations, increasing the temperature enhances the transport rate of water through the membrane, thereby improving the flux. This indicates that the membrane possesses a higher affinity for water, as the flux increases sharply with rising temperatures. In contrast, the negative activation energy for ethanol permeation indicates that transport is primarily governed by sorption rather than diffusion. Within the solution–diffusion model, the apparent activation energy reflects the combined contributions of diffusion and sorption. Because diffusion is always energetically activated, a negative value implies that exothermic sorption of ethanol within the polymer matrix outweighs the diffusion term. Mechanically, this behavior reflects the strong interaction between the polymer and ethanol, where the incorporation of Pebax into SA influences this process through mechanisms such as hydrogen bonding or dipole interactions, which stabilize ethanol molecules within the membrane at low temperatures. As temperature increases, these interactions weaken, reducing ethanol uptake and consequently permeability. This behavior reflects sorption-controlled transport, where membrane swelling and polymer–penetrant affinity play a more significant role than diffusion resistance in determining ethanol permeation.[62]

Fig. 17 shows that the total pervaporation flux decreases as the feed ethanol concentration increases, while the separation factor continues to rise. The separation factor reached 281 ± 1.11 with a flux of 133 ± 7.52 g m^{-2} h^{-1} at a feed concentration of 90 wt%. SA/Pebax membranes are hydrophilic, allowing small polar molecules like water to adsorb and diffuse much more easily than ethanol. As the ethanol concentration increases, the water fraction in the feed decreases, resulting in a decrease in the partial vapor pressure of water. Consequently, the partial vapor difference between the sides of the membrane becomes very small, causing the water permeation rate to decrease sharply.[63] Conversely, since the membrane is water-selective, the water to ethanol ratio in the permeate is high, thereby increasing the separation factor.

The comparative analysis presented in Table 3 highlights the performance of SA/Pebax composite membranes relative to other polymer-based and commercial membranes for water/ethanol pervaporation. The SA/Pebax (4 : 1) membrane developed in this study achieved a flux of 133 ± 7.52 g m^{-2} h^{-1} and a separation factor of 281 ± 1.11 at 50 °C, which represents a balanced performance under mild operating conditions. While this flux is lower than that of PEI/SA composites (1203 g m^{-2} h^{-1}) and layer-by-layer SA/PAH membranes (2020 g m^{-2} h^{-1}), those systems typically require higher temperatures (≥70 °C) or involve complex fabrication processes such as multilayer assembly, which limit scalability and increase production cost.

Commercial PERVAP™ membranes exhibit flux values near 1000 g m^{-2} h^{-1} but with modest separation factor (100–200),

Open Access Article. Published on 30 March 2026. Downloaded on 5/22/2026 11:10:49 PM. This article is licensed under a Creative Commons Attribution-NonCommercial 3.0 Unported Licence.

Table 3 Comparison of polymer based composite membranes for ethanol dehydration

Membrane types	Support type	Conditions	Flux (g m^{-2} h^{-1})	Separation factor (α)	Ref.
SA/Pebax (4 : 1)	Ceramic tubular	90 wt% EtOH, 50 °C	133 ± 7.52	281 ± 1.11	Current study
PEI/PVS	Ceramic tubular	94 wt% EtOH, 65 °C	18 400	8.2	Chen *et al.*[65]
SA	Ceramic tubular	75 wt% EtOH, 75 °C	1250	187	Ji *et al.*[66]
Layer-by-layer SA/PAH composite	Polymeric	90 wt% EtOH, 70 °C	2020	10 993	Sun *et al.*[67]
PDMS/MWCNT composite	Polymeric	90 wt% EtOH, 50 °C	420	6.25	Farahi *et al.*[68]
PEI/SA composite	Polymeric	90 wt% EtOH, 50 °C	1203	1542	Li *et al.*[21]
Commercial PERVAP™ membrane	Commercial (polymeric)	90 wt% EtOH, 60 °C	1000	100–200	Yave[69]

whereas PDMS/MWCNT composites show high flux but extremely low separation factor (α = 6.25), making them unsuitable for ethanol dehydration applications where water selectivity is critical. In contrast, the SA/Pebax membrane offers a significant improvement in selectivity compared to PDMS-based systems and provides a simpler fabrication route compared to layer-by-layer or inorganic membranes.

Another distinguishing feature of this work is the use of ceramic tubular supports, which confer superior mechanical strength and thermal stability compared to polymeric supports used in most benchmark membranes. This structural advantage enhances durability under industrial conditions and supports long-term operation without deformation or chemical degradation. Furthermore, the incorporation of Pebax and GA crosslinking ensures dimensional stability and mitigates swelling, addressing common limitations of biopolymer membranes. Previous study demonstrated that cross linked sodium alginate-based membranes had long term pervaporation stability over 30 h of the dehydration of ethanol (70 wt% water).[64] Future studies will focus on 24–72 h durability measurements to evaluate flux stability, separation-factor retention, and potential structural or swelling-related degradation under continuous pervaporation conditions.

Transport mechanism of ethanol–water dehydration

The transport mechanism in the SA/Pebax membrane is illustrated in Fig. 18. Mass transport in hydrophilic polymer blend membranes occurs *via* the solution–diffusion mechanism,[70] where the transport of liquid molecules is governed by the interactions between the penetrant molecules and the polymer chains.[71] Mass transport across the membrane proceeds in two distinct stages: selective sorption onto the membrane surface followed by molecular diffusion through the membrane matrix. SA is highly hydrophilic due to its abundant carboxyl and hydroxyl groups. Additionally, Pebax contains amide and ether segments that play a role in the solution–diffusion process. The ether segments act as flexible 'soft blocks' that permit the permeation of both water and alcohol molecules. Within these blocks, the difference in absorption rates depends solely on the diffusion coefficient, allowing smaller water molecules to diffuse faster than ethanol. Conversely, the amide segments function as rigid 'hard blocks' that restrict the movement of larger ethanol molecules, which are less polar than water. The amide groups engage in hydrogen bonding with water molecules specifically absorbed within the hard blocks, facilitating their transport to the permeate side.[71] Consequently, the SA/Pebax membrane preferentially adsorbs water molecules from

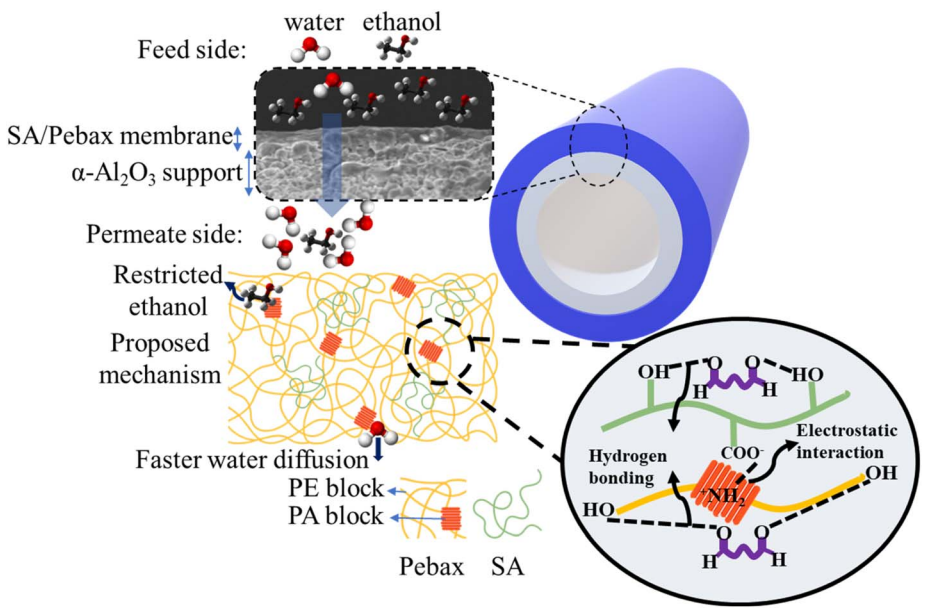

Fig. 18 SA/Pebax membrane transport mechanism in ethanol dehydration.

© 2026 The Author(s). Published by the Royal Society of Chemistry

Open Access Article. Published on 30 March 2026. Downloaded on 5/22/2026 11:10:49 PM. This article is licensed under a Creative Commons Attribution-NonCommercial 3.0 Unported Licence.

the ethanol–water feed and restricts the passage of ethanol through the membrane.

Conclusions

SA/Pebax composite membranes supported on ceramic tubes were successfully fabricated with varying blend ratios (5 : 1, 4 : 1, 3 : 1, and 3 : 2), and these variations significantly influenced structural, thermal, and separation properties. Incorporating Pebax into SA membranes markedly enhanced pervaporation performance for ethanol dehydration, primarily by improving thermal stability, mechanical strength, and dimensional integrity through GA crosslinking. Under optimized conditions (50 °C, 90 wt% ethanol feed), the SA/Pebax (4 : 1) membrane achieved a flux of 133 g m^{-2} h^{-1} and a separation factor of 281, representing a substantial improvement over pure SA membranes. At 50 °C demonstrated the optimal operating temperature owing to the balance between flux and separation factor performances. At this temperature, water transport is enhanced without causing excessive polymer relaxation, which would reduce the separation performance at higher temperatures. While total flux remains moderate compared to some other polymeric membranes, the combination of high selectivity, ceramic-supported robustness, and a simple, scalable fabrication process positions these membranes as promising candidates for energy-efficient ethanol–water separation in sustainable bioethanol production. Future work will focus on evaluating membrane reproducibility and long-term performance under continuous pervaporation conditions to ensure reliability for industrial applications.

Author contributions

Fadias Rara Ardana Lakuy: writing – original draft, investigation, conceptualization, data curation, visualization. Taufik Qodar Romadiansyah: methodology, conceptualization. Alvin Rahmad Widyanto: methodology, investigation, writing – review and editing, and visualization. Nur Lailiyah: writing – original draft, conceptualization. Resha Mutia Rahma: writing – original draft, editing. Riska Amelia: writing – original draft, conceptualization. Mikihiro Nomura: methodology, conceptualization, validation and resources. Triyanda Gunawan: investigation, resource. Zeni Rahmawati: conceptualization, investigation. Nurul Widiastuti: writing – review and editing, supervision, resources.

Conflicts of interest

The authors declare they have no known competing financial interests or personal relationships that could have appeared to influence the work reported in this paper.

Data availability

All data generated or analyzed during this study are included in this article.

Supplementary information (SI): the processed data of contact angle characterization, and swelling tests, and membrane performance. See DOI: https://doi.org/10.1039/d5ra09375a.

Acknowledgements

The authors gratefully acknowledge the financial support provided by the Directorate of Research and Community Service, Institut Teknologi Sepuluh Nopember, through the "Penelitian Keilmuan" (contract no. 1771/PKS/ITS/2025). In addition, Nur Lailiyah, Resha Mutia Rahma, and Riska Amelia would like to express their sincere appreciation to the Indonesia Endowment Fund for Education (Lembaga Pengelola Dana Pendidikan/LPDP) and the Ministry of Finance of the Republic of Indonesia for the scholarship support received.

References

1 T. J. Tse, D. J. Wiens and M. J. T. Reaney, *Fermentation*, 2021, **7**, 1–18.
2 S. S. Wirawan, H. Setiapraja, Mokhtar, A. Sugiyono, I. A. Ibadurrohman, N. P. Dian Nitamiwati and M. D. Solikhah, *Biomass Bioenergy*, 2025, **201**, 108112.
3 P. Peng, Y. Lan, L. Liang and K. Jia, *Biotechnol. Biofuels*, 2021, **14**, 1–33.
4 J. Baeyens, Q. Kang, L. Appels, R. Dewil, Y. Lv and T. Tan, *Prog. Energy Combust. Sci.*, 2015, **47**, 60–88.
5 H. Zentou, Z. Abidin, R. Yunus, D. Awang Biak and D. Korelskiy, *Processes*, 2019, **7**, 458.
6 B. A. Cinelli, D. M. G. Freire and F. A. Kronemberger, *Sep. Sci. Technol.*, 2019, **54**, 110–127.
7 A. R. Widyanto and M. Nomura, *Microporous Mesoporous Mater.*, 2026, **401**, 113956.
8 P. Aptel, N. Challard, J. Cuny and J. Neel, *J. Membr. Sci.*, 1976, **1**, 271–287.
9 K.-R. Lee, M.-J. Liu and J.-Y. Lai, *Sep. Sci. Technol.*, 1994, **29**, 119–134.
10 K. M. Song and W. H. Hong, *J. Membr. Sci.*, 1997, **123**, 27–33.
11 A. R. Widyanto, I. S. Caralin, N. Yuta and M. Nomura, *SEATUC J. Sci. Eng.*, 2025, **5**, 95–102.
12 G. Jyoti, A. Keshav and J. Anandkumar, *J. Eng.*, 2015, **2015**, 1–24.
13 W. Zhang, G. Li, Y. Fang and X. Wang, *J. Membr. Sci.*, 2007, **295**, 130–138.
14 L. Liang and E. Ruckenstein, *J. Membr. Sci.*, 1995, **106**, 167–182.
15 C. K. Yeom and K. H. Lee, *J. Membr. Sci.*, 1996, **109**, 257–265.
16 W. Cai, Q. Zhang, G. Q. Yang, H. Ye, M. Song and Z. Wang, *Mater. Today Commun.*, 2024, **40**, 109658.
17 C. K. Yeom and K. Lee, *J. Appl. Polym. Sci.*, 1998, **67**, 949–959.
18 D. A. Devi, B. Smitha, S. Sridhar, S. S. Jawalkar and T. M. Aminabhavi, *J. Chem. Technol. Biotechnol.*, 2007, **82**, 993–1003.
19 W. Kujawski, *Pol. J. Environ. Stud.*, 2000, **9**, 13–26.
20 W. F. Yong and H. Zhang, *Prog. Mater. Sci.*, 2021, **116**, 100713.

© 2026 The Author(s). Published by the Royal Society of Chemistry

Open Access Article. Published on 30 March 2026. Downloaded on 5/22/2026 11:10:49 PM. This article is licensed under a Creative Commons Attribution-NonCommercial 3.0 Unported Licence.

21 J. Li, X. Si, X. Li, N. Wang, Q. An and S. Ji, *Sep. Purif. Technol.*, 2018, **192**, 205–212.
22 R. Leo, G. Lecaros, S. Ho, H. Tsai, W. Hung, C. Hu, S. Huang, K. Lee and J. Lai, *Sep. Purif. Technol.*, 2021, **275**, 119125.
23 L. J. Fang, J. H. Chen, J. M. Wang, W. W. Lin, X. G. Lin, Q. J. Lin and Y. S. He, *ACS Omega*, 2021, **6**, 2675–2685.
24 S. E. Brady and D. R. Tyler, in *Molecular Design and Applications of Photofunctional Polymers and Materials*, The Royal Society of Chemistry, 2012, pp. 31–55.
25 P. Cai, J. Li, N. Zhang, D. Song, N. Wang and Q.-F. An, *J. Membr. Sci.*, 2023, **668**, 121254.
26 T. Jose, S. C. George and S. Thomas, in *Polymer Nanocomposite Membranes for Pervaporation*, Elsevier, 2020, pp. 1–16.
27 S. Sridhar, R. Suryamurali, B. Smitha and T. M. Aminabhavi, *Colloids Surf., A*, 2007, **297**, 267–274.
28 H. Nagar, C. Sumana, V. V. B. Rao and S. Sridhar, *J. Appl. Polym. Sci.*, 2017, **134**, 1–11.
29 M. Nikbakht Fini, S. Soroush and M. M. Montazer-Rahmati, *Membranes*, 2018, **8**, 119.
30 O. Myagmarjav, H. Noguchi, N. Tanaka, Y. Kamiji, C. Sugimoto, K. Ishii, M. Nomura and H. Takegami, *Int. J. Hydrogen Energy*, 2026, **198**, 152495.
31 H. Malektaj, A. D. Drozdov and J. deClaville Christiansen, *Int. J. Mol. Sci.*, 2023, **24**, 5064.
32 A. R. Widyanto and M. Nomura, *Membranes*, 2025, **15**, 355.
33 J. Yan, Y. Huang, D. B. Chrisey, J. Hu, X. Chen, J. Lin and M. Aprilliza, *IOP Conf. Ser.: Mater. Sci. Eng.*, 2017, **188**, 012019.
34 J. Tummachote, U. Mahanitipong, B. Rutnakornpituk and M. Rutnakornpituk, *Trends Sci.*, 2024, **21**, 7465.
35 A. F. Ismail, N. H. Othman and A. Mustafa, *J. Membr. Sci.*, 2009, **329**, 18–29.
36 H. R. Xie, C. H. Ji, S. M. Xue, Z. L. Xu, H. Yang and X. H. Ma, *Sep. Purif. Technol.*, 2018, **206**, 218–225.
37 S. K. Salestan, A. Rahimpour and R. Abedini, *Chem. Eng. Process.*, 2021, **163**, 108366.
38 M. Ehsan, H. Razzaq, S. Razzaque, M. Kanwal and I. Hussain, *J. Environ. Chem. Eng.*, 2023, **11**, 109185.
39 E. Seddigh, M. Azizi, E. S. Sani and D. Mohebbi-Kalhori, *Chin. J. Polym. Sci.*, 2014, **32**, 402–410.
40 S. N. A. Shafie, W. Y. Shen, J. J. Jaymon, N. A. H. M. Nordin, A. E. E. Mohamednour, M. R. Bilad, L. M. Kee, T. Matsuura, M. H. D. Othman, J. Jaafar and A. F. Ismail, *Membranes*, 2022, **12**, 414.
41 M. Ionita, M. A. Pandele and H. Iovu, *Carbohydr. Polym.*, 2013, **94**, 339–344.
42 A. R. Valagohar, S. A. Hashemifard and A. Khosravi, *Chem. Eng. Process.*, 2025, **210**, 110206.
43 J. Jiang, W. Cheng, Q. Tang, X. Pan, J. Li, L. Zhao, Z. Xi and W. Yuan, *Chin. J. Chem. Eng.*, 2023, **53**, 421–430.
44 G. Krausch, *Mater. Sci. Eng., R*, 1995, **14**, v–vi, 1–94.
45 S.-H. Hsu and W. M. Sigmund, *Langmuir*, 2010, **26**, 1504–1506.
46 K. Maghsoudi, G. Momen and R. Jafari, *Appl. Mater. Today*, 2023, **34**, 101893.
47 M. A. A. Hamid, Y. T. Chung, R. Rohani and M. U. M. Junaidi, *Sep. Purif. Technol.*, 2019, **209**, 598–607.
48 R. Castro-Muñoz and J. González-Valdez, *Molecules*, 2019, **24**, 3584.
49 P. Laurienzo, M. Malinconico, A. Motta and A. Vicinanza, *Carbohydr. Polym.*, 2005, **62**, 274–282.
50 C. G. Flores-Hernández, M. de los, A. Cornejo-Villegas, A. Moreno-Martell and A. Del Real, *Polymers*, 2021, **13**, 504.
51 Y. H. Liu, Y. Li, L. Yang, Y. Liu and L. Bai, *Polimery*, 2005, **50**, 37–42.
52 J. P. Soares, J. E. Santos, G. O. Chierice and E. T. G. Cavalheiro, *Eclética Quím.*, 2004, **29**, 57–64.
53 M. Eich, B. Reck, D. Y. Yoon, C. G. Willson and G. C. Bjorklund, *J. Appl. Phys.*, 1989, **66**, 3241–3247.
54 S. Meshkat, S. Kaliaguine and D. Rodrigue, *Sep. Purif. Technol.*, 2019, **212**, 901–912.
55 E. Parodi, L. E. Govaert and G. W. M. Peters, *Thermochim. Acta*, 2017, **657**, 110–122.
56 T. Eljaddi, J. Bouillon, D. Roizard and L. Lebrun, *Membranes*, 2022, **12**, 836.
57 M. N. Hyder, R. Y. M. Huang and P. Chen, *J. Membr. Sci.*, 2008, **318**, 387–396.
58 K. S. Burts, T. V. Plisko, V. G. Prozorovich, G. B. Melnikova, A. I. Ivanets and A. V. Bildyukevich, *Int. J. Mol. Sci.*, 2022, **23**, 7215.
59 M. S. A. Wahab and A. R. Sunarti, *Int. J. Membr. Sci. Technol.*, 2015, **2**, 78–84.
60 L. Yan, Y. S. Li, C. B. Xiang and S. Xianda, *J. Membr. Sci.*, 2006, **276**, 162–167.
61 S. Roy and N. R. Singha, *Membranes*, 2017, **7**, 53.
62 S. M. A. Z. Shawon, P. Fries, L. Xu, R. Wang, G. K. Jennings and S. Lin, *J. Membr. Sci.*, 2026, **738**, 124744.
63 Y. Huang, J. Ly, D. Nguyen and R. W. Baker, *Ind. Eng. Chem. Res.*, 2010, **49**, 12067–12073.
64 M. Dmitrenko, O. Mikhailovskaya, R. Dubovenko, A. Kuzminova, D. Myznikov, A. Mazur, K. Semenov, Y. Rusalev, A. Soldatov, S. Ermakov and A. Penkova, *Polymers*, 2024, **16**, 1206.
65 Y. Chen, F. Xiangli, W. Jin and N. Xu, *J. Membr. Sci.*, 2007, **302**, 78–86.
66 C.-H. Ji, S.-M. Xue and Z.-L. Xu, *ACS Appl. Mater. Interfaces*, 2016, **8**, 27243–27253.
67 Z. Sun, G. Zhao, G. Tang, Z. Zhao and P. Li, *Adv. Membr.*, 2025, **5**, 100132.
68 A. Farahi, G. D. Najafpour and A. Ghoreyshi, *Desalin. Water Treat.*, 2019, **137**, 300–311.
69 W. Yave, *J. Membr. Sci. Res.*, 2019, **5**, 216–221.
70 P. Kanti, K. Srigowri, J. Madhuri, B. Smitha and S. Sridhar, *Sep. Purif. Technol.*, 2004, **40**, 259–266.
71 S. Sridhar, S. Kalyani, Y. V. L. Ravikumar and T. S. V. N. Muralikrishna, *Sep. Sci. Technol.*, 2010, **45**, 322–330.

© 2026 The Author(s). Published by the Royal Society of Chemistry